A Metamaterial–Coupled Wireless Power Transfer System Based on Cubic High Dielectric Resonators

Rupam Das, Abdul Basir, and Hyoungsuk Yoo

***Abstract*—In this study, a metamaterial–coupled, highly–efficient, miniaturized, and long range Wireless Power Transfer (WPT) system based on a Cubic High Dielectric Resonator (CHDR) is explored. The proposed WPT system consists of two CHDR metamaterials separated by a distance and excited by two rectangular coils. Initially, this WPT system is analyzed by considering the cube dielectric permittivity, ε_r = 1000, and loss tangent, tanδ = 0.00001. From the Ansoft HFSS simulation, it is observed that the system operates in the hybrid resonance mode resonating as a horizontal magnetic dipole providing more than 90% power transfer efficiency at a distance of 0.1λ. In addition, parametric studies regarding the transmitter and receiver sizes, loss tangent, receiver misorientation, cube periodicity, etc. are carried out. One of the significant findings of this parametric study reveals that the suggested WPT system is less sensitive to the displacement of the receiver coil, and the WPT efficiency due to misorientation of the receiver can be increased by changing the CHDR cube rotation. Due to inaccessibility of the very high ε_r = 1000, eighteen microwave ceramic samples of EXXELIA TEMEX E5080 (Oxide composition: Ba Sm Ti) which has a permittivity, ε_r = 78, permeability, μ_r = 1, and a loss tangent, tanδ = 0.0004 was made for experimental verification. These cubes are surrounded by Teflon to make the CHDR resonators. From simulations and measurements, it is found that the proposed system outperforms the most recent high-dielectric or copper based WPT systems in terms of efficiency, range, size, and Specific Absorption Rate (SAR).**

***Index Terms*—Cubic high dielectric resonator, hybrid resonance mode, magnetic dipole, metamaterial, rectifier, specific absorption rate, wireless power transfer.**

I. Introduction

WIRELESS Power Transfer (WPT) makes it possible to supply power through an air gap, without the need for current-carrying wires [1]. WPT can provide power from an Alternating Current (AC) source to compatible batteries or devices without physical connectors or wires. WPT can recharge mobile phones and tablets [2], drones, cars, implantable devices [3], and even transportation equipment [4]–[5]. The concept of transferring power without wires, however, has been around since the late 1890s [6]. Since then, many research groups have been working on this problem, and different methodologies have been introduced to WPT systems. One of the issues being addressed is analyzing and optimizing the near-field inductive or magnetic resonate coupling WPT [7]–[10]. Another one is improving the power control capability and the WPT efficiency [11]–[18]. Miniaturization of the transmitter and receiver coil is also a major concern [3], [19]–[20]. Furthermore, a longer transfer distance and more flexible adaption are required for numerous mobile devices [9], [17], [20]–[21].

One of the non-radiative power transfer techniques is based on resonant coupling between the same-frequency resonators, where the power is transferred through the overlap of their near-fields. In 2007, a group from MIT experimentally transferred 60 W of power over a distance of 2 m with 45% efficiency *via* strongly coupled magnetic resonances between two metallic coils [7]. However, the resonance coupling based WPT system is very sensitive to the receiver and transmitter sizes, orientations and positions [22]–[23]. The possibility of omnidirectional WPT has also been explored, as opposed to the use of one direction or two directions on the same plane [24]. However, the proposed system in Ref. [24], yields only 60% efficiency at a distance of 0.013λ, which leaves much to be desired. Recently, WPT systems based on high permittivity dielectric resonators coupling have been experimentally tested [25]–[26]. As described in Ref. [25], this high permittivity dielectric introduced a higher order Magnetic Quadruple (MQ) mode which offers high WPT efficiency even with a random orientation between the transmitter and the receiver. The same group extended their work in another study [26] by incorporating a colossal permittivity dielectric (ε_r = 1000, tanδ = 0.00025) at 232 MHz. By applying an impedance matching technique, an efficiency of 50% was achieved within the separation between the resonators d = 16 cm (0.125λ).

To increase the power transfer efficiency, researchers have also demonstrated that a metamaterial (3D)/metasurface (2D) lens or slab can be used [13]–[14], [17]–[18], [21], [27]–[29]. Metamaterials (MTM) are artificial materials composed of engineered structures that possess peculiar electromagnetic properties not seen in natural materials, such as negative-refractive indexes and evanescent wave amplification [28], [30]. Bearing

Manuscript received June, 2018; revised September, 2018; accepted October, 2018. This work was supported by the Basic Science Research Program through the National Research Foundation of Korea funded by the Ministry of Education, Science and Technology under Grant 2016R1D1A1A09918140. (*Corresponding Author: Hyoungsuk Yoo.*)

The authors are with the Department of Biomedical Engineering, Hanyang University, Seoul, Republic of Korea. (e-mail: hsyoo@hanyang.ac.kr; rupamgump@gmail.com; engrobasir@gmail.com).

in mind that the magnetic resonant coupling based WPT is essentially coupling of evanescent waves, MTM can be used to enhance the WPT efficiency. On one hand, the efficiency of the WPT system with the MTM is considerably improved for adaptive charging. On the other hand, it can increase the flexibility of the operating range for telemetry systems, such as a farther transfer distance and larger misalignment tolerance for electronic or implantable devices [14]. In most previous studies [14], [17], [18], [21], [28], [29] a copper-based metamaterial/metasurface slab was placed between the transmitter and the receiver to improve the WPT system. However, the polarization dependence of the metamaterial poses a major drawback. Furthermore, copper-based metamaterials introduce ohmic losses at very high frequency and lower the quality factor (Q-factor) of the system as well as the efficiency. In contrast, resonant dielectric structures operating as Dielectric Resonator Antennas (DRAs) *via* displacement currents can be virtually free from ohmic loss, making them intrinsically highly efficient [25]–[26]. Furthermore, sub-wavelength DRAs with moderate permittivities ($\varepsilon_r > 5$) can efficiently support different modes of resonance [25]. One important and useful mode is pure magnetic resonance, which cannot be obtained with single-layer metallic resonators.

In this study, a metamaterial-coupled, highly-efficient, miniaturized, and long range WPT system based on Cubic High Dielectric Resonator (CHDR) is explored. The CHDR is a metamaterial with cubic high dielectric resonators in a cubic lattice embedded in a low dielectric background. This metamaterial was proposed by Kim *et al.* [31] in which the authors made use of a combination of Mie resonance and Bragg scattering to achieve the metamaterial properties [32]–[33]. Since, the efficiency of WPT systems has been improved with high permittivity dielectric coupling [26], and it is expected that the WPT efficiency can be further improved by using all-dielectric metamaterial coupling. To the best of our knowledge, there are no previous studies regarding high dielectric metamaterial–coupled WPT system. This paper is composed as follows. Section II analyzes the suggested WPT system by considering the unit cell of the CHDR, and CHDR metamaterial properties, and by characterizing the MTM-coupled WPT system. A comparison among previous studies and this study in terms of efficiency, WPT system size, and loss tangent variations is also included in this section. Parametric studies of the MTM-coupled WPT system are discussed. The influence on WPT efficiency owing to parameters such as the cube lattice periodicity, separation between the transmitter and CHDR, transmitter and receiver sizes, number of arrays, and receiver misalignment are addressed in Section III. Section IV comprises the experimental demonstration of the proposed WPT system. Two CHDR metamaterials were made by using eighteen high-dielectric cubes (ε_r = 78, tanδ = 0.0004) surrounded by Teflon. The Specific Absorption Rate (SAR) is numerically calculated and improvement in WPT efficiency in the presence of a saline phantom for the proposed WPT system is experimentally demonstrated. Finally, the versatility of the proposed WPT system is presented by taking into account the receiver misalignment.

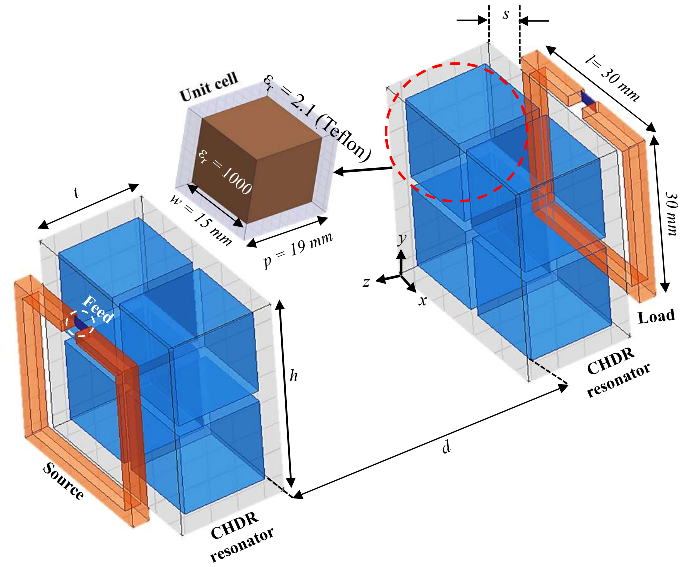

Fig. 1. (a) Schematic of the proposed CHDR metamaterial based WPT system.

II. Analysis of the Proposed WPT System

A schematic of the proposed WPT system is shown in Fig. 1. The system consists of two rectangular CHDR metamaterial resonators separated at a distance, d. For clarification, the WPT system will be divided into the following three sections: a) unit cell consideration, b) CHDR metamaterial characterization, and c) WPT system characterization.

A. Unit Cell Consideration

1) Theoretical Background: The proposed WPT system along with the unit cell of the CHDR structure are shown in Fig. 1. Theoretically, a rectangular cavity resonator with metal wall has the resonant frequencies given by:

$$f_{mnp} = \frac{1}{2\sqrt{\varepsilon\mu}}\sqrt{\left(\frac{m}{s}\right)^2 + \left(\frac{n}{t}\right)^2 + \left(\frac{p}{w}\right)^2}. \tag{1}$$

Where integers m, n, and p denote the number of half wave variations in the x, y, and z directions, respectively, and s, t, and w represent the dimensions of the rectangular cavity, respectively. If a cubic cavity resonator is chosen, then all lengths are equal, which means $s = t = w$. In case of a such cavity resonator, all the lowest order modes such as TM110, TE011, and TE101 have same field patterns or frequency, and referred as the degenerate modes. The resonant frequency of these degenerate modes is:

$$f = \frac{1}{\sqrt{2\varepsilon\mu}\, w}. \tag{2}$$

In case of a high dielectric resonator, boundary conditions at the walls can be considered as an open circuits [31], hence, resonant frequencies of the modes can also be approximated by Eqs. (1) and (2). It is found that if a unit cell simultaneously undergoes electric and magnetic resonances might demonstrate a polarization-invariant response due to superimposition of the two resonant modes [34]. The cubic high dielectric resonator has degenerate TE and TM modes due to cubic nature of

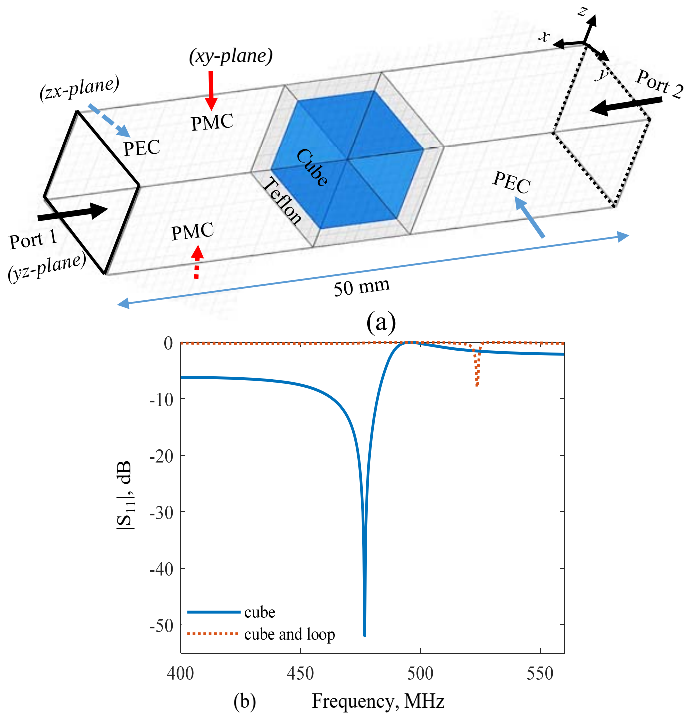

Fig. 2. (a) CHDR unit cell simulation setup. (b) Simulated reflection coefficient, $|S_{11}|$.

the 3D structure according to Eq. (1). Therefore, the CHDR is supposed to be less sensitive to the polarization of the incident wave in the z-direction (Fig. 1(a)). As a result, the proposed WPT system shows superior performance due to receiver misalignment, which will be addressed in the later section.

2) HFSS simulation: Initially, the cube size is chosen as w = 15 mm, having a permittivity ε_r = 1000, and tanδ = 0.00001. This high dielectric cube is surrounded by a low dielectric (ε_r = 2.1) Teflon substrate with a periodicity (or, lattice constant), p = 19 mm. The resonant frequency f of the lowest order modes for the above-mentioned CHDR resonators can be theoretically approximated based on the formulae given in Eq. (2), which gives us a resonant frequency of f = 447.1 MHz. To verify the theoretical approximation, an Ansys HFSS model is established, as shown in Fig. 2(a). Using the finite-element solver of HFSS, the resonant frequency (f) calculated under normal incidence. Taking advantage of the symmetry of the problem, the unit cell of the CHDR metamaterial was analyzed by applying two PMC and two PEC boundaries on the sides of the unit cell. The simulated resonant frequency was f = 476.8 MHz, which is very close to the calculated resonant frequency of f = 447.1 MHz according to the approximation in Eq. (2). The simulated reflection coefficient (S_{11}) is plotted and this plot indicates that, if a small loop is placed in the vicinity of the unit cell, f shifts to a higher frequency, as depicted in Fig. 2(b) .

B. CHDR Metamaterial Characterization

In general, CHDR metamaterials (MTM) are composed of periodic arrangements of high dielectric elements in a low dielectric background. The periodicity (p) of the unit cell controls the macroscopic resonance or the Bragg resonance, and the lattice resonance, whereas the microscopic resonance is due to the individual unit cell characteristics and is known as the Mie resonance. The combination of these two resonances give rise to a negative refractive index [35]. According to Fig. 1, two CHDR structures with height h = 36 mm, p = 19 mm, and thickness t = 19 mm made of a 2 $\times$ 2 array of high dielectric ceramic cube enclosed in a low dielectric (Teflon) background are considered. The MTM properties of the CHDR structure can be obtained by using a similar unit cell simulation setup (Fig. 2(a)), however, the unit cell should be replaced by the 2 $\times$ 2 CHDR array. The matrix elements S_{11}, S_{12}, S_{21}, and S_{22} are referred as the scattering parameters or the S-parameters. The parameters S_{11}, S_{22} have the meaning of reflection coefficients, and S_{12}, S_{21} define as the transmission coeffiecients. The S-parameters are related to both the refractive index (n) and the impedance (z). Therefore, extraction of parameters such as effective permittivity (ε_{eff}), effective permeability (μ_{eff}), and refractive index (n) are calculated based on the following equations [31]:

$$z = \pm\sqrt{\frac{(1+S_{11})^2 - S_{21}^2}{(1-S_{11})^2 - S_{21}^2}}, \tag{3}$$

$$e^{ink_o d} = \frac{S_{21}}{1 - S_{11}[(z-1)/(z+1)]}, \tag{4}$$

$$\varepsilon_{eff} = n/z, \quad and \quad \mu_{eff} = n \cdot z, \tag{5}$$

where, k_o and d denote the wave number and thickness of the metamaterial slab, respectively. The extracted real and imaginary parts of the effective permittivity and permeability are plotted in Fig. 3. A negative real part of either (or both) of these parameters enhances the evanescent wave amplification, whereas, the imaginary part controls the loss associated with the system [14]. Figs. 3(a) and (c) represent the real part, whereas Figs. 3(b) and (d) indicate the imaginary part of the effective permittivity and permeability, respectively. The region covered by the rectangular box is the negative refractive index region. In this portion of the plot, the real parts of both ε_{eff} and μ_{eff} become negative, and the imaginary parts are close to zero. Hence, the CHDR structure acts as a metamaterial with a negligible amount of loss.

C. MTM Coupled WPT System Characterization

To realize the WPT system, the CHDR metamaterial is excited by using a simple square loop. The loop has dimensions of 30 mm $\times$ 30 mm with a thickness of 3 mm, as shown in Fig. 1. A feed/port with an impedance of 50 Ω was placed in the loop and a separation of s = 4 mm was selected between the loop and the CHDR structure. The distance (d) between the CHDR was 50 mm ($\approx 0.1\lambda$, and more than three times higher than the cube size, w = 15 mm). Under the simulation setup shown in Fig. 1, resonance occurs around f = 560 MHz, which lies in the negative refractive index zone (rectangular box portion) of Fig. 3. The reflection (S_{11}) and the transmission (S_{21}) coefficients are plotted in Fig. 4(a). A maximum WPT efficiency (η) of more than 91% was found according to Fig.

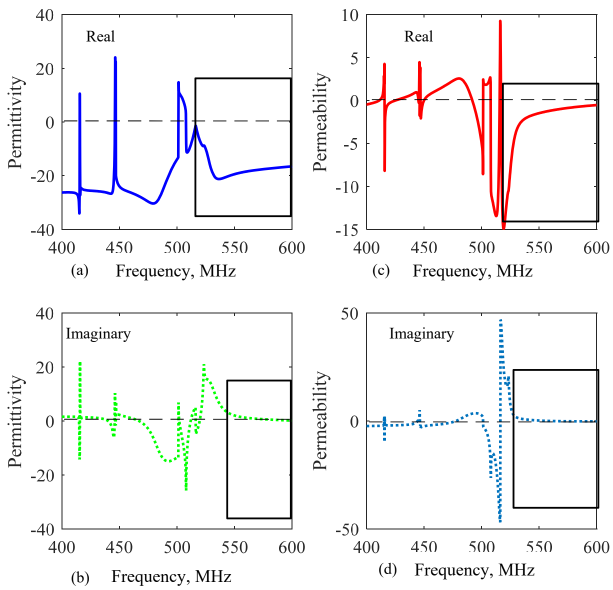

Fig. 3. Extracted parameter for the CHDR structure: (a) Real effective permittivity. (b) Imaginary effective permittivity. (c) Real effective permeability. (d) Imaginary effective permeability.

4(a), and η can be calculated based on the either of following equations [26]:

$$\eta = \frac{|S_{21}|^2}{1 - |S_{11}|^2}, \tag{6}$$

$$\eta = |S_{21}|^2. \tag{7}$$

In general, the WPT efficiency based on Eq. (6) approximates the maximum achievable WPT efficiency, whereas, Eq. (7) calculates the efficiency in a given situation. For a perfectly matched WPT system, Eqs. (6) and (7) yield an almost identical maximum WPT efficiency, as visualized in Fig. 4(a).

According to the Mie theory under a proper excitation, a high refractive index dielectric exhibits very strong magnetic resonances. Owing to the high dielectric contrast between free space and high dielectric, excitation of the CHDR resonator is expected to lead to strong localization of energy. To understand the above statement, the magnetic (H) and electric (E) field distributions are plotted in Fig. 4(b). As expected, the E and H fields are strongly confined in each cube inside the CHDR. The E field is swirling inside a CHDR cube, whereas, the H field, which lies perpendicular to E, is penetrating inside and out of the CHDR structure. The field distributions correspond to the hybrid resonance mode resonating as a horizontal magnetic dipole (MD) [36]–[37]. The hybrid resonance is one that is usually considered to originate from the very strong interactions between the elements in the unit cell [38]. In the plasmonic nano-structures, the horizontal magnetic–dipole–mode is used to build efficient surface plasmon polariton (SPP) couplers [36], whereas, in this study, this mode has been applied to introduce an efficient WPT system. Fig. 4(c) represents the horizontal magnetic ($|H|$) dipole coupling for the proposed system, hence, this is referred to as the MTM–MD–coupled WPT system.

The mechanism of the proposed system is distinct from prior resonance-based wireless powering systems (or resonant

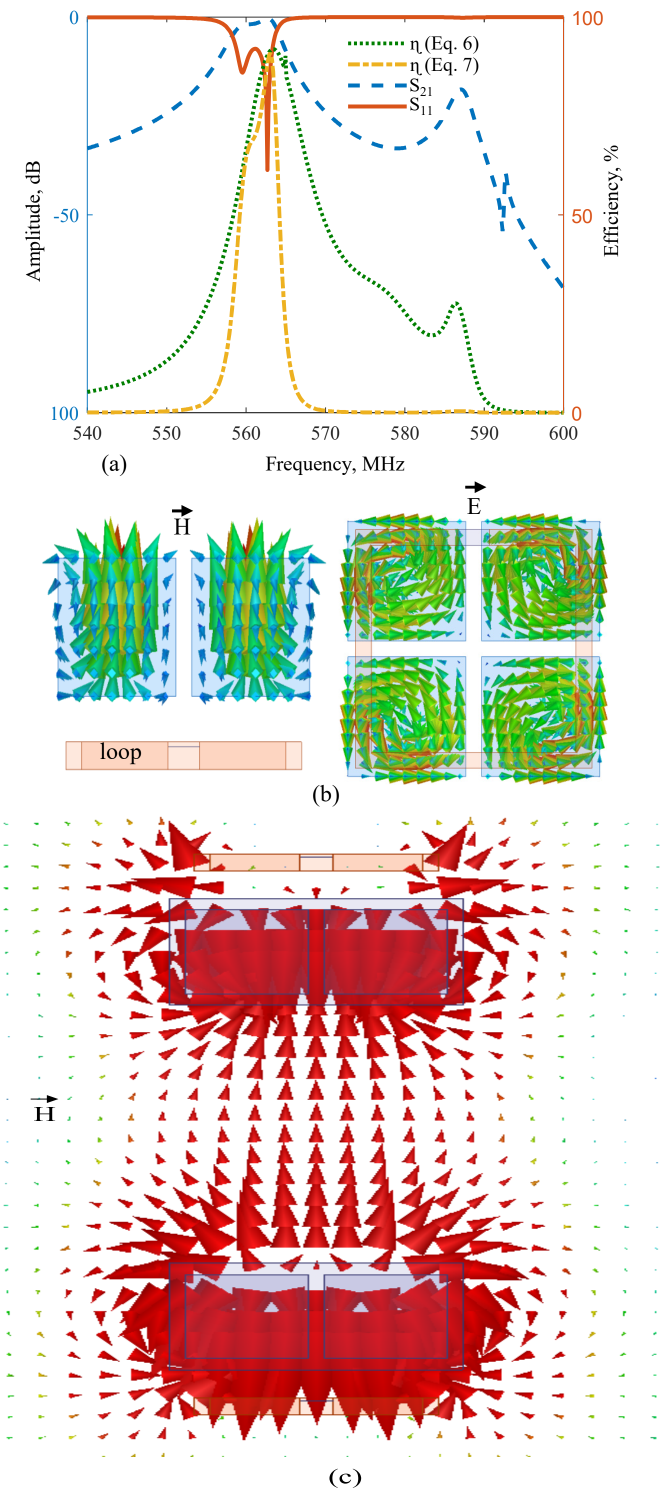

Fig. 4. (a) Characteristics of the proposed WPT system in terms of η, $|S_{11}|$, and $|S_{21}|$. (b) Magnetic ($|H|$) and electric ($|E|$) field distributions of the MTM-coupled WPT system. (c) Horizontal magnetic ($|H|$) dipole mode coupling for the proposed WPT system.

system with a metamaterial slab) in that energy is localized in modes intrinsic in dielectric objects rather than engineered resonances in objects such as coils or antennas. As magnetic field coupling occurs between two CHDR metamaterials, therefore, it is not necessary to design a sophisticated coil or antennas. We can use arbitrary non-resonant coils to excite or extract

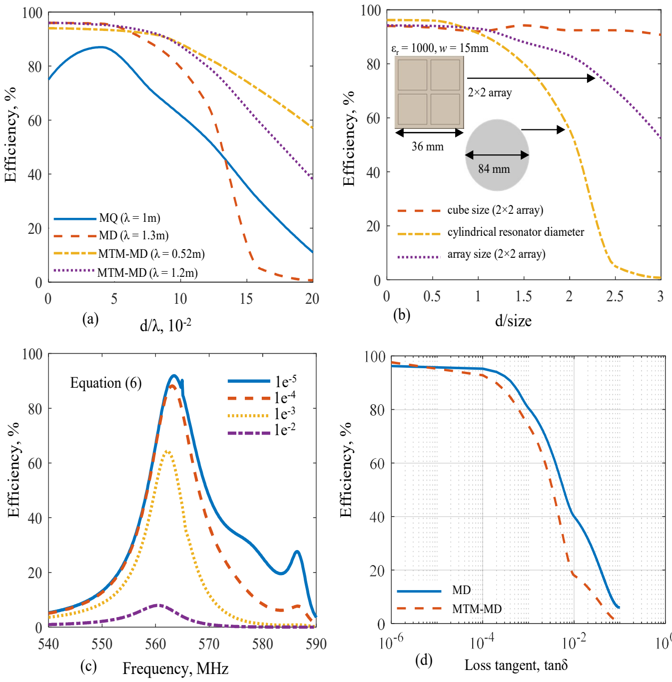

Fig. 5. Variations in η for different WPT systems when the distance is normalized by (a) Operational wavelength. (b) Array or dielectric size. (c) Variations in efficiency due to the loss tangent. (d) Comparison between the MTM–MD mode and the MD mode in terms of tanδ vs η.

the power. The reason is that the magnetic field produced by source coil (Fig. 1) can be drastically amplified by the transmitting MTM which couples with the receiving MTM to form a whole system behaving similarly to the conventional four–coil system [7]. The role of magnetic MTMs is that iy can largely weaken the fast divergence of the magnetic field–lines in the non–resonant coils [13].

A comparison among different WPT techniques is plotted in Fig. 5. The distance dependencies of the efficiency (η) for MQ [25], MD (tuned) [26], and MTM–MD modes are compared based on Eq. (6) and are represented in Fig. 5(a). It should be noted that, to compare each WPT system working at different frequencies, the distance (d) was normalized by the corresponding wavelengths (λ). For simplicity, the loss tangent, tanδ = 0.00001 was considered for all cases. In order to make a fair comparison in terms of λ for both the MD and MQ modes, the cube size and permittivity of the MTM-MD mode (Fig. 1) were adjusted to w = 25 mm and p = 29 mm, respectively, and ε_r = 2000. This setting gives an operational wavelength, $\lambda \approx$ 1.22 m for the MTM-MD mode. Fig. 5(a) indicates that, all the WPT systems exhibit a very good efficiency (90%) at short distances. However, it is obvious from Fig. 5(a) that the proposed MTM-MD based WPT system outperforms both the MD and MQ systems at long distances by a significant margin. Therefore, cascading small-sized multiple high-dielectric resonators, distributed with identical low-dielectric backgrounds, acts directly on the improvement of the evanescent wave coupling and decaying rate [39]. In addition, due to the“super-lens” effect (ε_{eff} = -1 or μ_{eff} = -1) of the CHDR structure as revealed in Fig. 2, the range of WPT systems is also improved [21].

It is well-known that the WPT efficiency in free space falls off rapidly when the operating distance (d) is larger than the largest size of the resonator [21]. Fig. 5(b) depicts the variations of η for different array and resonator sizes. The working WPT distance (d) was normalized by the associated array or resonator size. Considering only the cube size (w = 15 mm) and periodicity p = 19 mm, no significant difference in efficiency was observed. Nonetheless, in comparison with the size (diameter D = 84 mm) of the cylindrical resonator proposed in [26], the improvement in WPT efficiency for the CHDR MTM is noteworthy. Furthermore, when the whole 2 $\times$ 2 CHDR array size (length or width = 36 mm) is considered, the proposed CHDR MTM array still performs much better than the cylindrical resonator for the same normalized distance. Numerically, an efficiency of more than 75% can be obtained when the separation between the CHDRs is twice as much as the array size under the matched condition, which, in contrast, indicates a more than 50% improvement in the WPT efficiency to the study in [26].

The WPT system efficiency was obtained at tanδ = 0.00001, which is difficult to achieve in reality. Hence, variations of efficiency in terms of the loss tangent are indicated in Figs. 5(c) and (d) for both the MD and MTM–MD modes. For simulation, the distance d = 50 mm, and permittivity ε_r = 1000 were selected for each case. As expected from Fig. 5(c), a significant reduction in efficiency as well as in bandwidth occurs when the tangent loss increases. However, the drop of efficiency in the MTM–MD mode is higher than the MD mode according to Fig. 5(d), and the WPT efficiency is less than the 20%, even when tanδ = 0.01 for the MTM–MD mode. This is due to fact that the CHDR structure in the MTM–MD mode contains multiple small resonators, and losses in each resonator become significant when tanδ increases as compared to losses in a single dielectric resonator in the MD mode. Nonetheless, based on the high dielectric material used in [26], which has a permittivity of 1000 and a loss tangent of 2.5e^{-4} at 1 MHz, the proposed MTM–coupled WPT system is expected to have a maximum efficiency of more than 80% for the proposed MTM coupled WPT system at a distance of 0.1λ.

III. Parametric Study

According to Fig. 1, there are several parameters that can influence the performance of the proposed WPT system. It is obvious from Eq. (1) that, by increasing the permittivity (ε_r) and/or cube size (w), the resonance frequency can be reduced. Therefore, in this section, the effect of other parameters such as periodicity (p), separation (s), variations in the MTM array and transmitter/receiver size will be addressed. It is important to mention that, the effect of changing different parameters of the CHDR structure on the MTM properties are discussed in [31]. This study mainly focuses on the MTM-coupled WPT system, therefore, how the aforementioned parameters affect the whole WPT system (e.g., S_{11} and/or η) will be investigated.

A. Variation in Periodicity (p) and Separation (s)

Figs. 6(a) and (b) represent the variations in WPT efficiency due to changes in periodicity (p) and separation (s), and the

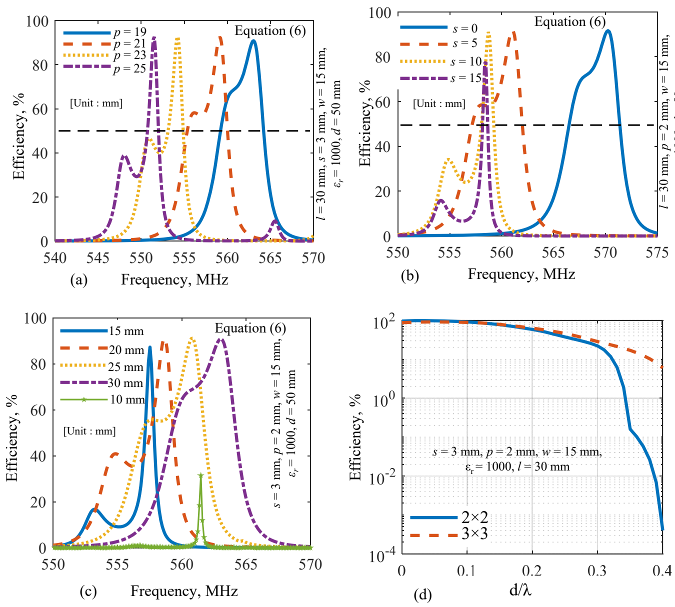

Fig. 6. Parametric studies and variations in: (a) Periodicity, p. (b) Separation, s. (c) Transmitter and receiver size, l. (d) Number of arrays.

corresponding simulation parameters are indicated in each plot. According to Fig. 6(a), when the periodicity (p) increases, the resonant frequency of the proposed WPT system shifts to a lower frequency, and the maximum η for each case remains almost the same. However, a reduction in WPT efficiency bandwidth (BW) was observed with increments in p. This reduction in BW is indicated by drawing a black dashed line along the x-axis at 50% WPT efficiency. Similar results were found due to a change in periodicity of the CHDR structure by *Kim et al.* Furthermore, the separation (s) between the transmitter/receiver and the CHDR also influences the resonant frequency and BW. Fig. 6(b) indicates that the resonant frequency of the proposed WPT system can be tuned by adjusting the distance (s) [26]. It is observed that, depending on the transmitter/receiver size (l), for each distance (d), there is an optimum separation (s), at which η is the maximum. Furthermore, the separation (s) is increased with an increasing distance (d), and the value of s should not be more than the resonator size (w) at short distances ($\leq 0.1\lambda$).

B. Variation in Transmitter/Receiver Size and Number of Arrays

It is important to minimize the transmitter/receiver size for various applications. As an example, nowadays, WPT in implantable devices is becoming more popular, which requires a smaller transmitter or receiver size. Variation in the transmitter and receiver size (length) as well as their corresponding efficiency is plotted in Fig. 6(c). It is interesting to observe that there is almost no change in the maximum efficiency ($\approx$ 90%) when both the transmitter and receiver length are gradually reduced from 30 mm to 15 mm. In addition, reduction in length of the excitation element also reduces the bandwidth as well as the resonant frequency. However, a notable altercation in resonant properties and reduction in efficiency were found as soon as the length decreases below 15 mm, which happens to

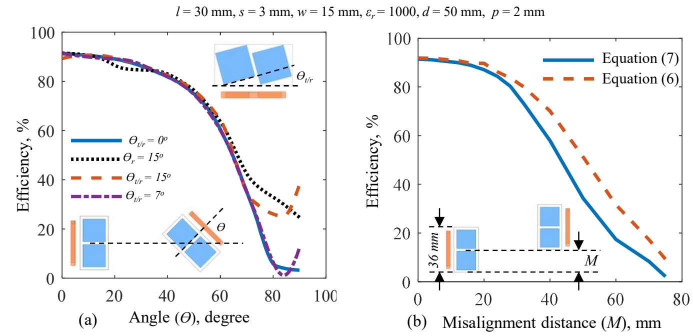

Fig. 7. Paramteric studies and variations in efficiency of the proposed WPT system due to: (a) Misorientation, θ. (b) Displacement, M.

be equal to the cube resonator length, w = 15 mm. Hence, the resonator size plays an important role in determining the maximum separation distance (s) and minimum transmitter/receiver size (l) to obtain the maximum WPT output for the proposed system. Another necessary parametric study is the number of MTM arrays, as it is significantly affects the power transfer distance. A comparison between 2 $\times$ 2 and 3 $\times$ 3 arrays is revealed in Fig. 6(d). According to this plot, the 3 $\times$ 3 array shows a significant improvement in η beyond the 0.3λ transfer distance as compared to the 2 $\times$ 2 array. This finding is identical to the study in [29]. As a consequence, the number of MTM arrays can be adjusted in accordance with the required transfer distance.

C. Receiver Misalignment

An efficient WPT system should be able to transfer power even if a misalignment exists between the transmitter and/or the receiver end. Depending on the misalignment susceptibility, the overall proficiency of a WPT system can be approximated. Here, the misalignment from the receiver end is considered. In general, two types of misplacement can occur, one is due to misorientation (θ) and the other is due to displacement (M), as visualized in Figs. 7a) and (b), respectively. According to Fig. 7(a), the maximum WPT efficiency of the proposed system remains at more than 50% at θ = 60^o, and decreases quickly to 3% for complete misorientation at θ = 90^o. However, a significant improvement in η was found when the MTM cubes are rotated along with θ. At first, only the receiver end cubes are rotated at an angle, θ_r = 15^o, which gives a noteworthy enhancement in efficiency when θ is more than 80^o. In addition, a rotation in the MTM cubes for both the transmitter and receiver ends ($\theta_{t/r}$) results in a remarkable boost in efficiency at θ = 90^o. Based on the simulated results, the maximum WPT efficiency can be more than 35% at θ = 90^o for $\theta_{t/r}$ = 15^o. As a consequence, the cube orientation ($\theta_{t/r}$) can be adjusted to obtain a reasonable amount of power transfer efficiency supposing a completely misoriented receiver end. Fig. 7(b) shows the change in η due to displacement M. It is interesting to see that, at a distance d = 50 mm, when the receiver end is entirely out of sight from the transmitter end (i.e., at M = 36 mm), this WPT system still maintains more than 50% efficiency, which implies a great susceptibility of the proposed WPT system to misalignments.

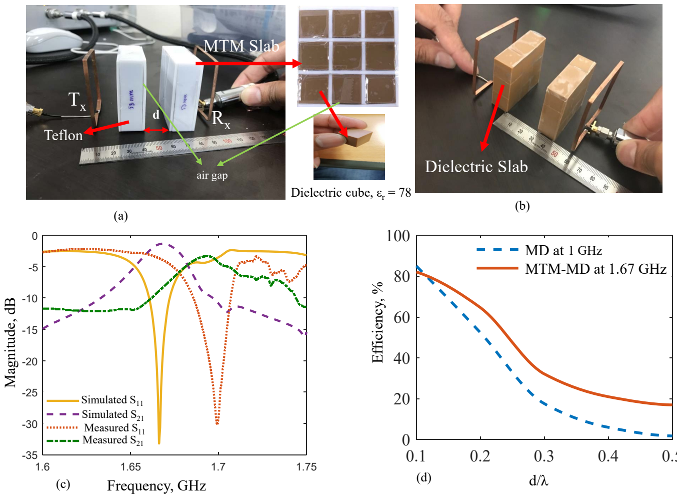

Fig. 8. (a) Photograph of the proposed MTM-MD WPT system along with the MTM slab. (b) Photograph of the MD based WPT system. (c) Simulated and measured S_{11} and S_{21} for the proposed WPT system at 0.1λ. (d) Variation in efficiency due to the working distance for the MTM–MD and MD based WPT systems.

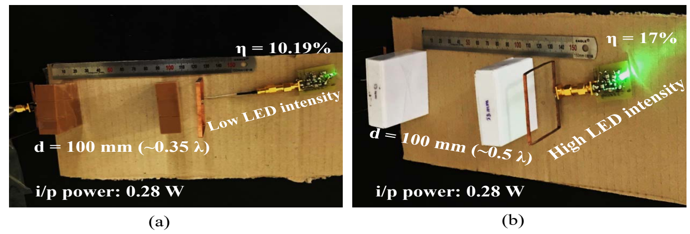

Fig. 9. Demonstration of the long range power transfer capability for (a) MD [26]. (b) MTM–MD WPT systems.

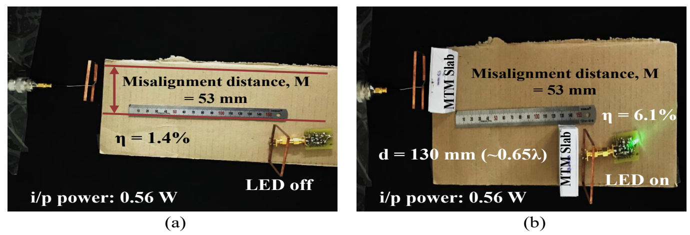

Fig. 10. Variation in efficiency due to Misalignment: (a) Traditional WPT system. (b) MTM–MD based WPT system.

IV. Experimental Verification of the Proposed WPT System

To validate the proposed method, the CHDR cube material was chosen as microwave ceramic samples of EXXELIA TEMEX E5080 along with a cube size w = 15 mm. Unfortunately, this ceramic only has a permittivity ε_r = 78, permeability, μ_r = 1, and a loss tangent tanδ = 0.0004. As a result, the resonant frequency was scaled up to higher frequencies (lower GHz range). Fig. 8(a) shows a photograph of the experimental setup along with metamaterial slabs. It should be noted that at high frequency, loss increases and the evanescent wave decays more rapidly. Hence, instead of using a 2 $\times$ 2 array, a 3 $\times$ 3 array is used, and the size of the transmitter (T_x) and receiver (R_x) loop also increased accordingly to achieve the proper S_{11}. For measurements, two identical 3 $\times$ 3 CHDR metamaterials having dimensions of 53 mm $\times$ 53 mm $\times$ 19 mm are separated by a distance d and excited by two similar rectangular loops of dimensions 50 mm $\times$ 50 mm. The thickness of the loop was 0.5 mm. The periodicity p and the separation s were selected as 19 mm and 15 mm, respectively. In addition, to make a fair comparison between the recently introduced MD based WPT systems and the proposed WPT system, the MD WPT system [26] was created by combining all the available cubes to act as a dielectric slab, as shown in Fig. 8(b). From simulation, the resonant frequencies for the MD and MTM-MD modes were found as 1 GHz and 1.67 GHz, respectively. The simulated and measured reflection (S_{11}) and transmission coefficients (S_{21}) for the MTM-MD WPT system are plotted in Fig. 8(c). The measured resonance frequency was found at 1.7 GHz, and the maximum S_{21} measured as -2.43 dB as compared to the simulated S_{21} of -1.3 dB at d = 20 mm (0.1λ). The deviation between the simulated and measured results mainly occurs due to the presence of a visible air gap between cubes and Teflon. This air gap influences the performance of the MTM slab and coupling. The mismatch between the T_x and R_x loop also affected the measured results. Considering all these experimental limitations, the measured results remain almost identical to the simulated results. For ε_r = 78, efficiency vs. distance variations is plotted in Fig. 8(d). The efficiency was calculated based on Eq. (5), and the working WPT distance (d) was normalized by the associated wavelength (λ). The results in Fig. 8(d) matched the results predicted in Fig. 5(a), where both WPT systems achieve 80% efficiency within a short distance. However, for the same normalized distance, the MTM–MD based WPT system achieves a higher efficiency at long distances (0.3λ or more) as compared to the MD based WPT system. To illustrate this, a green LED is connected *via* a rectifier to the receiver end for both cases and a working WPT distance was chosen as d = 100 mm.

Fig. 9 demonstrates and compares the performance of the MTM-MD and MD WPT systems at d = 100 mm. For the same power input from the power amplifier, the intensity of the LED for the proposed WPT system is higher than the MD based WPT system. The performance of both systems in terms of efficiency and operational wavelength is also indicated in Fig. 9. It is obvious from this demonstration that the proposed WPT system is highly efficient at short distances and can be applied for long range power transfer. Furthermore, a comparison table among previous studies and the proposed WPT system is shown in Table I. This comparison testifies that the MTM-MD based WPT systems are not only superior in terms of η improvement and transfer distance, but the proposed method also requires lower transmitter and receiver sizes, thus establishing the idea of a metamaterial–coupled, highly–efficient, miniaturized, and long range WPT system.

For a versatile WPT system, misalignment and misorientation of T_x/R_x should also be evaluated. The effect of receiver misalignment on the WPT efficiency is addressed in detail in Section III. Experimentally, a demonstration of misalignment was examined by introducing displacement M in the R_x end, as shown in Fig. 10. The displacement M is selected as 53

TABLE I
COMAPRISON OF THE PROPOSED WPT SYSTEM WITH PREVIOUS WORKS

Ref.	Operating Frequency	Tx Size	Rx Size	Transfer Distance (d)	MTM or Dielectric Size	S_{21} Improvement (dB)	η Improvement
[7]	10 MHz	$\pi \times 60 \times 60$ cm^2	$\pi \times 60 \times 60$ cm^2	200 cm (0.06λ)	–	–	45%
[13]	23.4 MHz	7.8 $\times$ 7.8 cm^2	7.8 $\times$ 7.8 cm^2	7 cm (0.0055λ)	7.8 $\times$ 7.8 cm^2	–	5% to 40%
[17]	27 MHz	$\pi \times 2.5 \times 2.5$ cm^2	$\pi \times 1.8 \times 1.8$ cm^2	5 cm (0.0045λ)	6.9 $\times$ 6.9 cm^2	-9.47 to -7.4	11.3% to 18.2%
[18]	6.78 MHz	15 $\times$ 15 cm^2	15 $\times$ 15 cm^2	30 cm (0.0068λ)	18.6 $\times$ 18.6 cm^2	-23 to -18.9	0.5% to 1.3%
[28]	27.1 MHz	$\pi \times 20 \times 20$ cm^2	$\pi \times 20 \times 20$ cm^2	50 cm (0.045λ)	58.5 $\times$ 58.5 cm^2	-7.68 to -3.28	17% to 47%
[29]	6.3 MHz	$\pi \times 25 \times 25$ cm^2	$\pi \times 25 \times 25$ cm^2	100 cm (0.02λ)	70 $\times$ 70 cm^2	-7 to -2.65	19.9% to 54.3%
[26]	232 MHz	$\pi \times 3.6 \times 3.6$ cm^2	$\pi \times 3.6 \times 3.6$ cm^2	16 cm (0.124λ)	$\pi \times 3.7 \times 3.7$ cm^2	–	50%
[This Work: ε_r = 1000 (Simulation)]	560 MHz	3 $\times$ 3 cm^2	3 $\times$ 3 cm^2	10 cm (0.19λ)	3.6 $\times$ 3.6 cm^2	–	58.5% (Eq. 5)
[This Work: ε_r = 78 (Measured)]	1.7 GHz	5 $\times$ 5 cm^2	5 $\times$ 5 cm^2	3.6 cm (0.2λ)	5.3 $\times$ 5.3 cm^2	–	52% (Eq. 5)

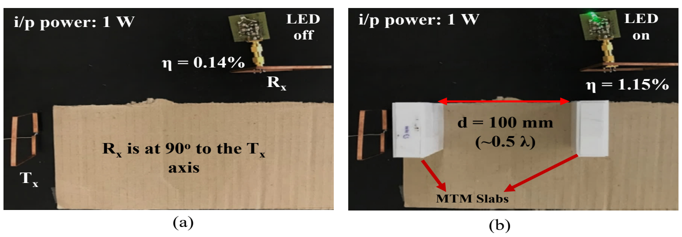

Fig. 11. Demonstration of WPT efficiency considering the worst case scenario of 's': (a) Traditional WPT. (b) MTM-MD WPT systems.

mm. The distance, d is chosen as 130 mm, and more than 5% efficiency was achieved for the MTM-MD case at a distance of 0.65λ even when the R_x end is completely out of sight from the T_x end. However, the received η reduced to 1.4% without the MTM coupling. By doubling the input power compared to Fig. 9, the received power without MTM not enough to turn on the LED, as indicated in Fig. 10(a). In contrast, by simply placing the MTMs for the same input power, the LED shines brightly, as revealed in Fig. 10(b). This illustration provides insight into the power transfer capability of the proposed WPT system for misalignments.

In the MTM-MD based WPT system the large separation (s) also signifies that magnetic field coupling occurs between the two MTM resonators, therefore, T_x and R_x can be moved independently. This phenomenon is displayed in Fig. 11, where R_x is placed at the worst position possible, with complete displacement to the T_x axis and rotated by 90^o. For d = 100 mm (0.5λ), traditional WPT gives a negligible transfer efficiency of 0.14% as opposed to the 1.15% for the proposed WPT system. These results are also reflected by Figs. 11(a) and (b) for the power input of 1 W. This separation 's' feature enables future studies where, there will be no need to place the devices (R_x end) on a charging pad for wireless charging. Instead, we will be able to establish truly wireless charging as long as the devices remain in the MTM–coupled region.

The Specific Absorprtion Rate (SAR) still remains a concern with the WPT system [40]–[41]. If any human tissue/implantable device lies in the middle of T_x and the R_x,

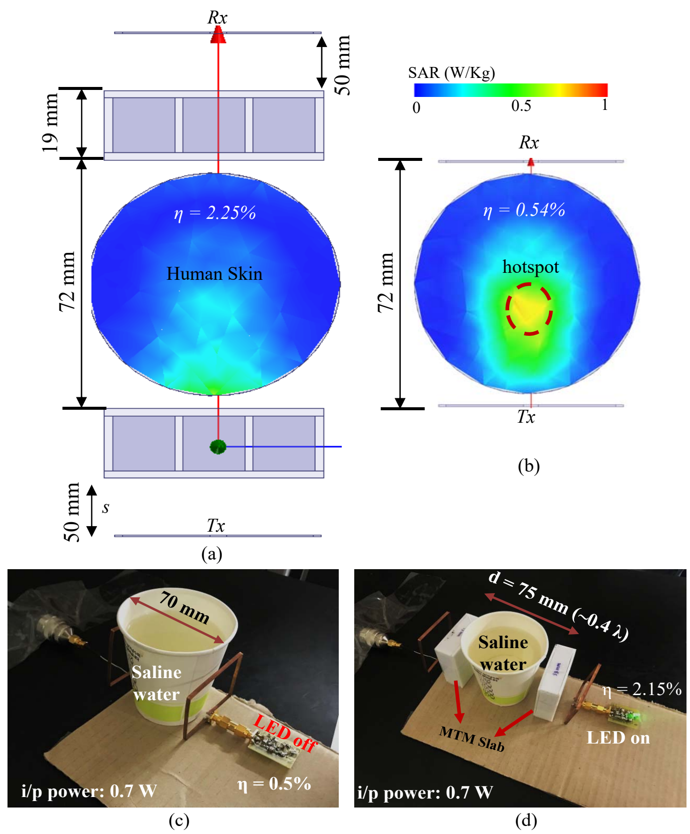

Fig. 12. Normalized 1-g local SAR calculation in human skin tissue for: (a) MTM–MD based WPT system. (b) Traditional inductive coupling based WPT system. Measurements in a simple cup containing fresh water for (c) Traditional WPT system. (d) Proposed MTM–MD system.

it may be exposed to the electromagnetic fields produced by the WPT system, thus, causing tissue heating or implant damage. This exposure or SAR limit is defined by the ICNIRP guidelines [41] recommend that whole body SAR does not exceed 0.08 W/kg and 10-g SAR does not exceed 2 W/kg for the head and the trunk, and 4 W/kg for limbs. In this study, the separation (s) between the T_x/R_x and the MTM slab (see Fig. 1) plays an important role to reduce the SAR.

The parameter, 's' can be adjusted for tuning the WPT system and to optimize the WPT efficiency, as discussed in Section III. A of the main manuscript. It is also mentioned that for optimizing efficiency, 's' can be increased with an increasing distance d. This situation has many advantages. In one case, the proposed method can reduce the SAR as well as increase the efficiency compared to the most commonly used inductive/resonant coupling. A HFSS simulation illustration of the SAR is shown in Fig. 12. For the simulation setup, a cylindrical skin phantom (ε_r = 39.2, σ = 1.11 at 1.7 GHz) of radius 3 cm and height 5.3 cm is placed in between the transmitter and receiver side, and the distance, d was chosen as 72 mm. Two similar rectangular loops of dimension 50 mm $\times$ 50 mm were considered as T_x and R_x. For Simplicity, simulated 1–g SAR was normalized to 1 W/kg. As visualized in Fig. 12(b), in traditional inductive coupling if the exciting element (i.e., T_x) lies very close to human tissue, it introduces a local hot spot inside the tissue, as opposed to the MTM-coupled WPT system in Fig. 12(a). In addition, it is important to note that the simulated received efficiency is almost four times higher in the case of the proposed WPT system as compared to the traditional WPT system, even when the T_x and the R_x are more than 20 cm apart from each other. Measurement validation is carried out by placing a simple cup of fresh water as a phantom in the middle of T_x and R_x separated by 70 mm, as indicated in Fig. 12(c). From Figs. 12(c) and (d), it can be confirmed that, for the same power input of 0.7 W, the MTM-MD based WPT system offers higher η as compared to the traditional WPT system, as indicated by the LED. Due to low SAR and high η in the MTM–MD WPT system, the input power can also be increased to reach the SAR safety limit when more power is required by a system.

V. Conclusion

In this paper, a WPT system referred to as 'MTM–MD', based on two CHDR metamaterials which are excited by two similar non–resonant oops, is explored. The CHDR metamaterial is composed of an array of cubic high dielectrics arranged in a low dielectric background. From HFSS simulation, it is observed that this WPT system introduces a horizontal magnetic dipole between the CHDR metamaterials and achieves more than 80% efficiency at short distances and 50% efficiency at a distance of 0.2λ. The proposed WPT system requires a smaller foot-print for higher efficiency compared to previous studies and the transmitter and receiver sizes should not be lower than the CHDR's cube size for a reasonable WPT efficiency. It is also found that a larger CHDR array helps to improve the range of the WPT system. For measurements, the CHDR metamaterials were designed by considering microwave ceramic samples of EXXELIA TEMEX E5080 for high dielectric cubes and Teflon was selected as a low dielectric background. Experimental comparison between the most recent high–dielectric–coupled WPT system and the proposed system was also carried out to demonstrate the long range power transfer capability. The versatility of the system was also discussed by considering the receiver misalignment. We found that the suggested WPT system can withstand receiver displacement from the transmitter axis as well as the orientation of the cubes inside the CHDR metamaterial can be adjusted for misorientation while maintaining an efficient WPT system. Furthermore, the MTM-MD WPT system performed superiorly in the presence of a tissue like material in terms of the SAR and efficiency as compared to the traditional WPT system. Due to the heterogeneous nature of the human tissues, it is expected that the proposed dielectric–based method will only expose or stimulate the desired part without affecting the surrounding media. Hence, the proposed concept can be explored to power up a tiny medical device or to give tissue-specific heating for hyperthermia without affecting the surrounding tissues and so on.

References

[1] S. Y. R. Hui, W. Zhong, and C. K. Lee, "A Critical Review of Recent Progress in Mid-Range Wireless Power Transfer," *IEEE Trans. Power Electron.*, vol. 29, no. 9, pp.4500–4511, Sep. 2014. DOI 10.1109/TPEL.2013.2249670.

[2] S. Y. Hui, "Planar Wireless Charging Technology for Portable Electronic Products and Qi," in *Proc. IEEE*, vol. 101, pp. 1290–1301, Jun. 2013. DOI 10.1109/JPROC.2013.2246531.

[3] J. S. Ho. A. J. Yeh, E. Neoftou, S. Kim, Y. Tanabe, B. Patolla, R. E. Beygui, and A. S. Y. Poon, 'Wireless power transfer to deep-tissue microimplants," in *Proc. Natl. Acad. Sci. U.S.A.*, vol. 111, no. 22, pp. 7974–7979, Jun. 2014. DOI 10.1073/pnas.1403002111.

[4] C. C. Mi, G. Buja, S. Y. Choi, and C. T. Rim, "Modern advances in wireless power transfer systems for roadway powered electric vehicles," *IEEE Trans. Ind. Electron.*, vol. 63, no. 10, pp. 6533–6545, Oct. 2016. DOI 10.1109/TIE.2016.2574993.

[5] J. Shin, S. Shin, Y. Kim, S. Ahn, S. Lee, G. Jung, S. J. Jeon, and D. H. Cho, "Design and Implementation of Shaped Magnetic-Resonance-Based Wireless Power Transfer System for Roadway-Powered Moving Electric Vehicles," *IEEE Trans. Ind. Electron.*, vol. 61, no. 3, pp.1179–1192, Mar. 2014. DOI 10.1109/TIE.2013.2258294.

[6] N. Tesla, "Apparatus for transmitting electrical energy," Dec. 1 1914, US Patent 1,119,732. [Online]. Available: https://www.google.com/patents/US1119732.

[7] A. Kurs, A. Karalis, R. Moffatt, J. D. Joannopoulos, P. Fisher, and M. Soljacic, "Wireless Power Transfer via Strongly Coupled Magnetic Resonances," *Science*, vol. 317, pp. 83–86, Jul. 2007. DOI 10.1126/science.1143254.

[8] J. Zhang, X. Yuan, C.Wang, and Y. He, "Comparative analysis of two-coil and three-coil structures for wireless power transfer," *IEEE Trans. Power Electron.*, vol. 32, no. 1, pp. 341–352, Jan. 2017. DOI 10.1109/TPEL.2016.2526780.

[9] A. P. Sample, D. T. Meyer, and J. R. Smith, "Analysis, experimental results, and range adaptation of magnetically coupled resonators for wireless power transfer," *IEEE Trans. Ind. Electron.*, vol. 58, no. 2, pp. 544–554, Feb. 2011. DOI 10.1109/TIE.2010.2046002.

[10] B. L. Cannon, J. F. Hoburg, and D. D. Stancil, "Magnetic resonant coupling as a potential means for wireless power transfer to multiple small receivers," *IEEE Trans. Power Electron.*, vol. 24, no. 7, pp.1819–1825, Jul. 2009. DOI 10.1109/TPEL.2009.2017195.

[11] W. Zhong and S. Y. R. Hui, "Charging time control of wireless power transfer systems without using mutual coupling information and wireless communication system," *IEEE Trans. Ind. Electron.*,vol. 64, no. 1, pp. 228–235, Jan. 2017. DOI 10.1109/TIE.2016.2598725.

[12] N. L. Zhen, R. A. Chinga, and R. Tseng, "Design and test of a high-power high-efficiency loosely coupled planar wireless power transfer system," *IEEE Trans. Ind. Electron.*, vol. 56, no. 5, pp. 1801–1812, May 2009. DOI 10.1109/TIE.2008.2010110.

[13] Q. Wu, *et al.,* "Wireless power transfer based on magnetic metamaterials consisting of assembled ultra-subwavelength meta-atoms," *EPL*, vol. 109, no. 6, Mar. 2015. DOI 10.1209/0295-5075/109/68005.

[14] L. Li, H. Liu. H. Zhang, and W. Xue, "Efficient Wireless Power Transfer System Integrating With Metasurface for Biological Applications," *IEEE Trans. Ind. Electron.*, vol. 65, no. 4, pp. 3230–3239, Apr. 2018. DOI 10.1109/TIE.2017.2756580.

[15] Y. J. Kim, D. Ha, W. J. Chappell, and P. P. Irazoqui, "Selective wireless power transfer for smart power distribution in a miniature-sized multiple receiver system," *IEEE Trans. Ind. Electron.*,vol. 63, no. 3, pp. 1853–1862, Mar. 2016. DOI 10.1109/TIE.2015.2493142.
[16] M. Zargham and P. G. Gulak, "Maximum achievable efficiency in nearfield coupled power-transfer systems," *IEEE Trans. Biomed. Circuits Syst.*, vol. 6, no. 3, pp. 228–245, Jun. 2012.. DOI 10.1109/TBCAS.2011.2174794.
[17] A. Rajagopalan, A. K. RamRakhyani, D. Schurig, and G. Lazzi, "Improving power transfer efficiency of a short-range telemetry system using compact metamaterials," *IEEE Trans. Microw. Theory Techn.*, vol. 62, no. 4, pp. 947–955, Apr. 2014. DOI 10.1109/TMTT.2014.2304927.
[18] Y. Cho *et al.*, "Thin PCB-type metamaterials for improved efficiency and reduced EMF Leakage in wireless power transfer systems," *IEEE Trans. Microw. Theory Techn.*, vol. 64, no. 2, pp. 353–364, Feb. 2016. DOI 10.1109/TMTT.2015.2514090.
[19] D. R. Agrawal *et al.*, "Conformal phased surfaces for wireless powering of bioelectronic microdevices," *Nat. Biomed. Eng.*, vol. 1, no. 0043, Mar. 2017. DOI 10.1038/s41551-017-0043.
[20] S. Du, D. Ha, E. K. Chan, B. Wen, J. Hong, H. Widmer, and C. E. Wheatley, "Wireless Power Transfer Using Oscillating Magnets," *IEEE Trans. Ind. Electron.*, vol. 65, no. 8, pp. 6259–6269, Aug. 2018. DOI 10.1109/TIE.2017.2786289.
[21] G. Lipworth *et al.*, "Magnetic Metamaterial Superlens for Increased Range Wireless Power Transfer," *Sci. Rep.*, vol. 4, no. 3642, Jan. 2014. DOI 10.1038/srep03642.
[22] D. Liu, H. Hu, and S. V. Georgakopoulos, "Misalignment sensitivity of strongly coupled wireless power transfer systems," *IEEE Trans. Power Electron.*, vol. 32, no. 7, pp. 5509–5519, Jul. 2017. DOI 10.1109/TPEL.2016.2605698.
[23] J. P. K. Sampath, A. Alphones, and D. M. Vilathgamuwa, "Figure of merit for the optimization of wireless power transfer system against misalignment tolerance," *IEEE Trans. Power Electron.*, vol. 32, no. 6, pp. 4359–4369, Jun. 2017. DOI 10.1109/TPEL.2016.2601939.
[24] N. H. Van and C. Seo "Analytical and Experimental Investigations of Omnidirectional Wireless Power Transfer Using a Cubic Transmitter," *IEEE Trans. Ind. Electron.*, vol. 65, no. 2, pp. 1358–1366, Feb. 2018. DOI 10.1109/TIE.2017.2733470.
[25] M. Song, I. Iorsh, P. Kapitanova, E. Nenasheva, and P. Belov, "Wireless power transfer based on magnetic quadrupole coupling in dielectric resonators," *Appl. Phys. Lett.*, vol. 108, no. 023902, Jan. 2016. DOI/10.1063/1.4939789.
[26] M. Song, P. Belov, and P. Kapitanova, "Wireless power transfer based on dielectric resonators with colossal permittivity," *Appl. Phys. Lett.*, vol. 109, no. 223902, Dec. 2016. DOI/10.1063/1.4971185.
[27] M. C. K. Wiltshire, J. B. Pendry, I. R. Young, D. J. Larkman, D. J. Gilderdale, and J. V. Hajnal, "Microstructured magnetic materials for RF flux guides in magnetic resonance imaging," *Science.*, vol. 291, no. 5505, pp. 849–851, Feb. 2001. DOI/10.1126/science.291.5505.849.
[28] B. Wang, K. H. Teo, T. Nishino, W. Yerazunis, J. Barnwell, and J. Zhang, "Experiments on wireless power transfer with metamaterials," *Appl. Phys. Lett.*, vol. 98, no. 254101, Jun. 2011. DOI/10.1063/1.3601927.
[29] A. L. A. K. Ranaweera, T. P. Duong, and J. W. Lee, "Experimental investigation of compact metamaterial for high efficiency mid-range wireless power transfer applications," *J. Appl. Phys.*, vol. 116, no. 043914, Jul. 2014. DOI/10.1063/1.4891715.
[30] D. R. Smith, J. B. Pendry, M. C. K. Wiltshire, "Metamaterials and Negative Refractive Index," *Science.*, vol. 305, no. 5685, pp. 788–792, Aug. 2004. DOI/10.1126/science.1096796.
[31] J. Kim and A. Gopinath, "Simulation of a metamaterial containing cubic high dielectric resonators," *Phys. Rev. B.*, vol. 76, no. 115126, Sep. 2007. DOI/10.1103/PhysRevB.76.115126.
[32] S. O'Brien and J. B. Pendry, "Photonic band-gap effects and magnetic activity in dielectric composites," *J. Phys.: Condens. Matter*, vol. 14, pp. 4035–4044, Apr. 2002. DOI/JPhysCM/14/4035.
[33] E. Cubukcu, K. Aydin, E. Ozbay, S. Foteinopoulou, and C. M. Soukoulis, "Electromagnetic waves: Negative refraction by photonic crystals," *Nature*, vol. 423, pp. 604–605, Jun. 2003. DOI/10.1038/423604b.
[34] K. Agarwal, C. Liu, D. Joung, H. R. Park, J. Jeong, D. S. Kim, and J. Cho, "Three-Dimensionally Coupled THz Octagrams as Isotropic Metamaterials," *ACS Photonics*, vol. 4, pp. 2436–2445, Sep. 2017. DOI/10.1021/acsphotonics.7b00617.
[35] R. Das and H. Yoo, "Application of a Compact Electromagnetic Bandgap Array in a Phone Case for Suppression of Mobile Phone Radiation Exposure," *IEEE Trans. Microw. Theory Tech.*,vol. 66, no. 5, May 2018. DOI 10.1109/TMTT.2017.2786287.
[36] C. Zou, W. Withayachumnankul, M. Bhaskaran, S. Sriram, and C. Fumeaux, "Dielectric Resonator Nanoantennas: A Review of the Theoretical Background, Design Examples, Prospects, and Challenges," *IEEE Antennas Propag. Mag.*, vol. 59, no. 6, pp. 30–42, Dec. 2017. DOI 10.1109/MAP.2017.2752638.
[37] A. Petosa, *Dielectric Resonator Antenna Handbook*, Norwood, MA: Artech House, 1997.
[38] A. N. Serdyukov, I. V. Semchenko, S. A. Tretyakov, and A. Sihvola, *Electromagnetics of Bi-anisotropic Materials: Theory and Application*, Amsterdam, Gordon and Breach Science, 2001.
[39] R. Castro-Beltran, N. Huby, G. Loas, H. Lhermite, D. Pluchon, and B. Beche, "Improvement of efficient coupling and optical resonances by using taper-waveguides coupled to cascade of UV210 polymer microresonators," *J. Micromech. Microeng.*, vol. 24, no. 12, 125006 (7pp), Nov. 2014. DOI 10.1088/0960-1317/24/12/125006.
[40] R. L. McIntosh, V. Anderson, R. J. McKenzie, "A numerical evaluation of SAR distribution and temperature changes around a metallic plate in the head of a RF exposed worker," *Bioelectromagnetics*, vol. 26, no. 5, pp. 377–388, May. 2005. DOI 10.1002/bem.20112.
[41] Guidelines for limiting exposure to time-varying electric, magnetic, and electromagnetic fields (up to 300 GHz). International Commission on Non-Ionizing Radiation Protection. ICNIRP, *Health Phys.*, vol. 75, no. 4, Oct. 1998. https://www.icnirp.org/cms/upload/publications/ICNIRPemfgdl.pdf

Rupam Das received the B.Sc. degree in electrical and electronics engineering from the Chittagong University of Engineering and Technology, Chittagong, Bangladesh, in 2011, and the M.Sc. and Ph.D. degrees in Biomedical engineering from the University of Ulsan, Ulsan, South Korea, in 2013 and 2017, respectively. He is currently a Post–Doctoral Associate of biomedical engineering with the Hanyang University. His current research interests include implantable antennas and devices, wireless power transfer, metamaterial, electromagnetic band gap structures, and magnetic resonance imaging safety.

Abdul Basir is a student member of IEEE. He received his B. Sc. degree in Telecommunication Engineering from the University of Engineering and Technology, Peshawar, Pakistan in 2015. Currently, he is pursuing his MS leading to Ph.D. in Biomedical Engineering at the Hanyang University, Seoul, South Korea. His research interests include implantable antennas and systems, biomedical circuits, wearable antennas, MIMO communication, metamaterial, dielectric resonator antennas, reconfigurable antennas, long range wireless power transfer, and wireless charging of biomedical implants.

Hyoungsuk Yoo received the B.Sc. degree in electrical engineering from Kyungpook National University, Daegu, South Korea, in 2003, and the M.Sc. and Ph.D. degrees in electrical engineering from the University of Minnesota, Minneapolis, MN, USA, in 2006 and 2009, respectively. In 2009, he joined the Center for Magnetic Resonance Research, University of Minnesota, as a Post-Doctoral Associate. In 2010, he joined Cardiac Rhythm Disease Management, Medtronic, MN, USA, as a Senior MRI Scientist. From 2011 to 2018, he was an Associate Professor with the Department of Biomedical Engineering, School of Electrical Engineering, University of Ulsan, Ulsan, South Korea. Since 2018, he has been an Associate Professor with the Department of Biomedical Engineering, Hanyang University, Seoul, South Korea. His current research interests include electromagnetic theory, numerical methods in electromagnetics, metamaterials, antennas, implantable devices, and magnetic resonance imaging in high-magnetic field systems. He is the CEO of E2MR, start up company since 2017.